



## Classification of Alzheimer Disease with Molecular Communication Systems using LSTM

Ibrahim ISIK<sup>1\*</sup>

<sup>1</sup>Department of Electrical Electronics Engineering, Inonu University, 44280, Malatya, Turkey

\* Corresponding Author : [ibrahim.isik@inonu.edu.tr](mailto:ibrahim.isik@inonu.edu.tr) ORCID: 0000-0003-1355-9420

### Article Info:

DOI: 10.22399/ijcesen.1061006

Received : 21 January 2022

Accepted : 30 March 2022

### Keywords

Nano communication  
Number of received molecule  
Deep learning  
LSTM

### Abstract:

Today, there are many diseases caused by cell or inter molecular communication. For example, a communication disorder in the nerve nano-network can cause very serious nervous system-related diseases such as Multiple Sclerosis (MS), Alzheimer's and Paralysis. Understanding these diseases caused by communication is very important in order to develop innovative treatment methods inspired by information technologies. In addition, many advanced environmental and industrial nano-sensor networks such as the development of biologically inspired Molecular Communication systems (MCs), cellular-accurate health monitoring systems, many medical applications such as the development of communication-capable nano-implants for nervous system diseases. Nano networks focused on communication between nano-sized devices (Nano Machines) is a new communication concept which is known as MCs in literature. In this study, on the contrary to the literature, a new Long Short-Term Memory (LSTM) based MC model has been used to analyse the proposed system. After obtained the number of received molecules for different number of Amyloid Beta ( $A\beta$ ) which causes Alzheimer's, a new method based on the LSTM model of deep learning is used for the classification of  $A\beta$ . Finally it is obtained that when the number of  $A\beta$  increases, the number of received molecules decrease. On a data set with five classes, experiments are conducted using LSTM. The proposed model's precision, accuracy and sensitivity values are determined as 97.05, 98.59 and 98.54 percent, respectively. The categorization procedure of the findings generated from the designed model appears to be performing well.

## 1. Introduction

In Molecular communication systems (MCs), chemical transceiver may be more favorable for implementation issues in transmitting information from transmitter to receiver or vice versa. In several fields, such as dentistry, bio-medical, environmental monitoring, industrial and defense purposes, these models can be used. Nearly all biological cells on their receiver surface use receptors to receive proteins, nutrients or other substances. A lot of studies have been carried out about the communication of nano-devices in recent years [1-6]. Generally, the transmitter (Tx) and receiver (Rx) parts are investigated to analyze transmitted and received molecules in a fluid media such as channel transfer function and the number of

received molecules with a point transmitter and fully and half fully absorbing spherical receiver, pulse peak time and pulse amplitude concerning for the distance between transmitter and receiver, and attenuation, propagation delay, receptor models which are placed on the receiver randomly are considered as antenna using graphene and carbon nanotubes due to their prominent sensing capabilities for fixed Rx and Tx model of molecular communication via diffusion (MCvD) systems [7,8]. In [9], the proposed MCs model is analyzed for different distance values between Tx-Rx nanomachines and the diffusion constant of the environment. It is concluded from the study that, the number of received molecules increases with increasing diffusion constant and a decreasing distance between Tx and Rx. In [10], an adaptive

threshold mechanism, signal to interference, and bit alignment scheme are investigated for a simple and effective demodulation scheme for a mobile receiver with a speed of drift  $V = 7.9 \times 10^{-4} \text{ m/s}$  and diffusion coefficient of  $D = 2.42 \times 10^{-10} \text{ m}^2/\text{s}$ . The parameters such as the ratio of flow and receiver velocity and symbol interval are analyzed in terms of bit error rate (BER) using a fixed transmitter and mobile receiver. BER with or without ISI mitigation for different transmitting intervals is calculated and analyzed in this study [10]. The communication distance, which is described in MC systems as the distance between nanomachines, is one of the critical parameters that have a major impact on the quality of communication efficiency. In fixed MC, for instance, the CIR is defined as the expected number of molecules received, depending on the distance between nanomachines. The receiver can predict CIR and set an effective detection threshold in advance with knowledge of distance. The distance calculation and developing a mechanism between nanomachines should therefore be a primary justification for the design of MC systems using a neural networks or deep neural networks [11-14]. The hitting probability of transmitted molecules is generally analyzed at the receiver part in literature. The probability of a molecule being transmitted in a 1-D system is as follows:

$$f_{hit}^{1D}(t) = \frac{d}{\sqrt{4\pi Dt^3}} e^{-\frac{d^2}{4Dt}}, \quad (1)$$

$$f_{hit}^{3D}(t) = \frac{r_r}{d+r_r} \frac{d}{\sqrt{4\pi Dt^3}} e^{-\frac{d^2}{4Dt}}, \quad (2)$$

where  $r_r$  and  $d$  show the radius of the receiver, and distance from the transmitter to the surface of receiver, respectively.

In this study, firstly, the proposed MCs model is analyzed on the molecule reception rate of the model for different number of A $\beta$  values separately. Secondly, after the number of received molecules is obtained for different number of A $\beta$ , a new method based on the Long Short-Term Memory (LSTM) model of deep learning is used for the classification of number of A $\beta$ .

## 2. Materials and Methods

Amyloid peptide is a protein produced by the cell itself in order to maintain its vital activities. However, with the breakdown of this protein by various enzymes, deterioration of the cell structure or overproduction, diseases for which no cure has yet been found arise. The most well-known of these is Alzheimer's disease, which causes forgetfulness

in humans [14,15]. It is estimated that Alzheimer's disease is a disease caused by miscommunication or inability of cells to communicate. Amyloid beta (A $\beta$ ) peptides are formed by the degradation of amyloid precursor proteins (app), known as type 1 membrane protein, by  $\beta$ -secretase and  $\gamma$ -secretase enzymes [15]. It is known that App is produced by many cells of living things, but precursor proteins produced by nerve cells in the brain cause Alzheimer's disease [14,15]. Molecular communication is being studied by many researchers within the scope of nano-bio systems in order to shed light on the treatment of diseases caused by the disruption of communication systems of these and similar cells [16]. Although it is not known exactly how the communication between cells is disrupted in the literature, as a result of some experimental studies on mice, it has been concluded that the A $\beta$  40-42 peptide accumulates between neurons more than normal and prevents the transfer of information from the donor to the receiver [17].

In this study, pure diffusive channel method is used for moving of NMs in the fluid media. [18-20]. A point transmitter, sphere receiver, transporting molecules, and receptors on the receiver make up the suggested MCs model. Between the transmitter and the receiver, MMs are used as information carriers as shown in Fig. 1. In a 3-D environment, the receiver is set at the origin (0, 0, 0) and the transmitter is randomly placed at a distance  $d$  from the receiver. Every time step, the position of the receiver is changed at random, while the position of the transmitter is changed after each bit duration. A fluid propagation medium surrounds both the transmitter and the receiver. The medium is thought to be unconstrained, allowing it to spread in all directions to infinity. After being discharged into the medium, where they propagate according to Brownian motion, the molecules may arrive at the receiver. The information molecules are absorbed by the spherical receiver's receptors with a radius of  $r$  s. The receiver absorbs a molecule that collides with one of the receptors on its surface. It bounces back if it collides with the receiver's surface without striking a receptor [21,22]. For the sake of simplicity, the suggested model ignores messenger molecule collisions, as stated in the literature. The cumulative number of received molecules for a spherical completely absorbing receiver is calculated analytically in Eq. 3. The absorption probability of a chemical in transition is presented in 3-D environment without taking into account the influence of receptors by the completely absorbing receiver until time  $t$ .

$$F_{hit}(t) = \frac{r_r}{r_0} \operatorname{erfc}\left(\frac{d}{\sqrt{4Dt}}\right), \quad (3)$$

where  $r_0$  denotes the distance between the point transmitter and the receiver's center,  $t$  is the time after the molecule was released, and  $\operatorname{erfc}()$  denotes the complementary error function [21].

**Table 1.** System parameters.

Radius of receiver, $r_r$	3.101 $\mu\text{m}$
Number of $A\beta$	5, 10, 15, 20 $\mu\text{m}$
Radius of receptor, $r_s$	0.01 $\mu\text{m}$
Number of receptor	7200
Number of transmitted molecules	20000
Number of simulation	100

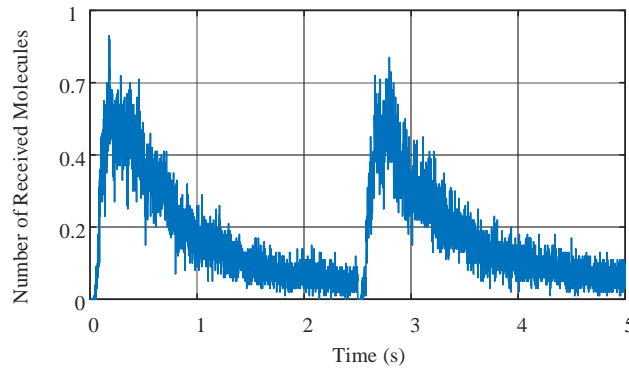
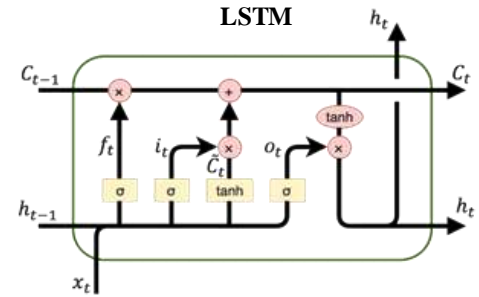
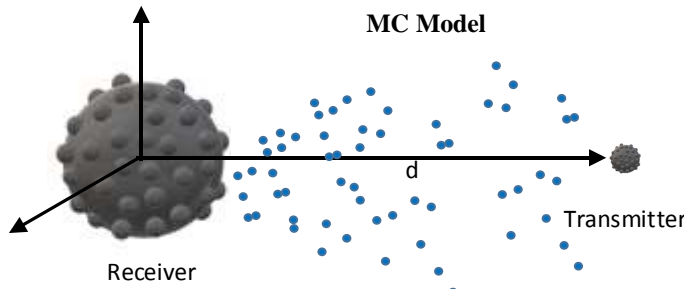


**Figure 1.** The proposed MC model with LSTM.

As shown in Eq. 4, the first step in processing an LSTM network is to determine the information to be taken from the cell (table 1). The sigmoid function awarded the data definition and exclusion process. The sigmoid function also determined which portion of the mine's output should be extracted. The forget gate layer, also known as  $f_t$ , is a sigmoid layer that makes this decision: where  $h(t-1)$  is a vector that goes from 0 to 1 for each integer in the cell state  $C_{(t-1)}$ .

$$f_t = \sigma(W_F[h_{t-1}, X_t] + b_f) \quad (4)$$

where  $(W_F)$  and  $(b_f)$  are the weighting matrices of the forget gate and bias vector, respectively, and is the sigmoid function. The input gate of the LSTM

Diffusion constant of environment, $D$	79.4 $\mu\text{m}^2/\text{s}$
----------------------------------------	-------------------------------

## 2.1 Long Short-Term Memory (LSTM)

Long Short-Term Memory (LSTM) networks are a form of Recurrent Neural Networks (RNN) [23]. The hidden layer of an LSTM neural network, also known as the LSTM cell, has a complex structure. As illustrated in Fig. 1, the LSTM cell is made up of three gates: the input gate, the forget gate, and the output gate [23,25], which control the flow of information through the cell and neural network. The LSTM model shown in figure 1, is a chain-like structure built of progressively constructed data [26,27].

is described in Eqs. 5-7. In Eq. 5, the new information ( $X_t$ ) from the input gate layer is stored, and the cell state is also updated. There are two components to this. The "input gate layer," a sigmoid layer, chose which values would update or not (0 or 1), and the second layer is known as tanh. The tanh function in Eq. 6 produced a vector for the new candidate value (-1 to 1) and applied weight to the data provided (to push the values between 1 and 1). To update the new cell state, two values are multiplied. The following stages are to update the old memory state,  $C_{t-1}$ , into the new memory state,  $C_t$ , as shown in Eq. 7.

$$i_t = \sigma(W_i[h_{t-1}, X_t + b_i]), \quad (5)$$

$$N_t = \tanh(W_n[h_{t-1}, X_t] + b_n), \quad (6)$$

$$C_t = C_{t-1}f_t + N_t i_t. \quad (7)$$

The cell states  $C_{(t-1)}$  and  $C_t$  in the time interval between  $t-1$  and  $t$  are  $C_{(t-1)}$  and  $C_t$ , respectively. In Eq. 8, the sigmoid layer determined which parts of the current cell reach the output. The output of the sigmoid gate ( $O_t$ ) is then multiplied by the new values ( $C_t$ ) formed by the tanh layer, as shown in Eq. 9.

$$O_t = \sigma(W_o[h_{t-1}, X_t] + b_o) \quad (8)$$

$$h_t = O_t \tanh(C_t) \quad (9)$$

$W_o$  and  $b_o$  which are the weight matrix and bias vector of the output gate respectively.

The accuracy, precision, and sensitivity of the results obtained from the suggested method were assessed using assessment criteria. Eqs. 10-12 give the mathematical formulae for each of these evaluation criteria.

$$Accuracy = \frac{|TP|+|TN|}{|TP|+|FP|+|FN|+|TN|} \quad (10)$$

$$Precision = \frac{|TP|}{|TP|+|FP|} \quad (11)$$

$$Sensitivity = \frac{|TP|}{|TP|+|FN|} \quad (12)$$

In this study, the proposed methodology and main components for the classification of number of  $A\beta$  are analysed in detail. The number of  $A\beta$ , time and number of received molecule features are given as input to the LSTM model and then the specifications obtained from LSTM were classified by using Softmax.

### 3. Results

The recommended model is examined using MATLAB 2021. A PC with an Intel I95.1GHz processor, 64GB of memory, and an NVIDIA Quadro RTX 3000 GPU was also used to train and test the recommended model. The time, number of  $A\beta$ , and number of received molecules are given as inputs to the created two-layer LSTM model with 32 and 64 outputs. Figure 2 shows the fluctuation of LSTM features in two-dimensional coordinates (x and y), which represent two of the LSTM characteristics.

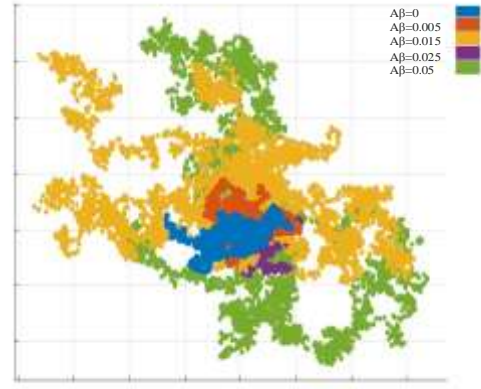


Figure 2. 2D Representation of LSTM Features.

Half of the data is utilized for training and half is used for testing in the first trial. In the second trial, the data is separated for testing and training using the 10-fold cross validation process. Many parameters are used during the training phase to guarantee that the model is adequate and optimal. The measurements are carried out with varied batch sizes and learning rates for the optimum results. 32, 64, and 128 batch sizes have been chosen. The learning rates are also chosen as 0.1, 0.01, and 0.001 respectively. The epoch has been changed from 50 to 50. The accuracy and loss during training and testing are depicted in Figure 3.

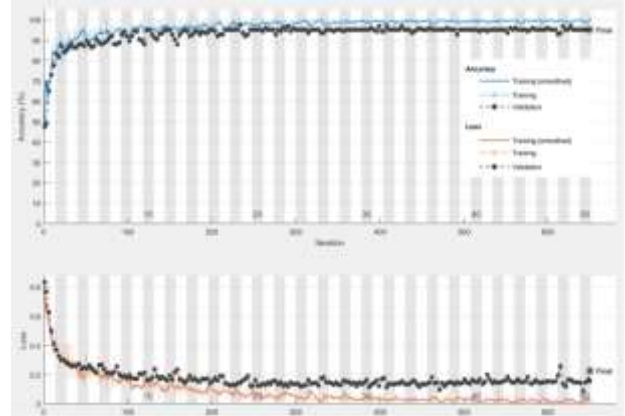


Figure 3. Plots of accuracy and loss on training and validation sets.

Table 2 shows the categorization results obtained by employing 50 percent for training and 50 percent for testing. The greatest accuracy of 97.05 percent is attained when the batch sizes are set to 128 and the learning rate is set to 0.001. The batch sizes were set to 64 and the learning rate was 0.1, yielding the maximum accuracy of 96.12 percent, and the batch sizes were set to 32 and the learning rate was 0.001, yielding the best accuracy of 96.14 percent.

**Table 2.** Classification results obtained by splitting the data into 50% training and 50% test.

	Batch-Size	Learning rate	Accuracy %	Precision %	Sensitivity %
LSTM		0.1	95.79	96.02	96.54
	32	0.01	95.59	96.02	95.82
		0.001	96.14	96.42	94.23
		0.1	96.12	96.68	96.52
	64	0.01	95.59	95.54	98.54
		0.001	95.41	96.92	97.50
		0.1	96.85	97.50	97.97
	128	0.01	95.92	97.90	96.98
		0.001	97.05	98.59	97.01

Table 3 displays the classification results obtained by utilizing the 10-k fold cross validation procedure to divide the data. When the batch sizes are set to 64 and the learning rate is set to 0.001, the maximum accuracy is achieved. The batch sizes were 32 and the learning rate was 0.001, resulting in a maximum accuracy of 97.99 percent, while the batch sizes were 128 and the learning rate was 0.01, resulting in the greatest accuracy of 97.75 percent. The confusion matrix and Receiver Operating Characteristic (ROC) curve for the best classification result are shown in Figures 4 and 5.

**Table 3.** Classification results obtained by dividing the data with the 10-fold cross validation technique.

	Batch-Size	Learning rate	Accuracy %	Precision %	Sensitivity %
LSTM		0.1	96.92	96.92	96.42
	32	0.01	96.88	97.79	95.29
		0.001	97.99	96.34	94.99
		0.1	96.66	97.39	99.09
	64	0.01	96.81	97.81	95.07
		0.001	98.57	96.54	96.90
		0.1	97.45	97.36	97.03
	128	0.01	97.75	97.53	96.14
		0.001	96.06	96.86	95.01

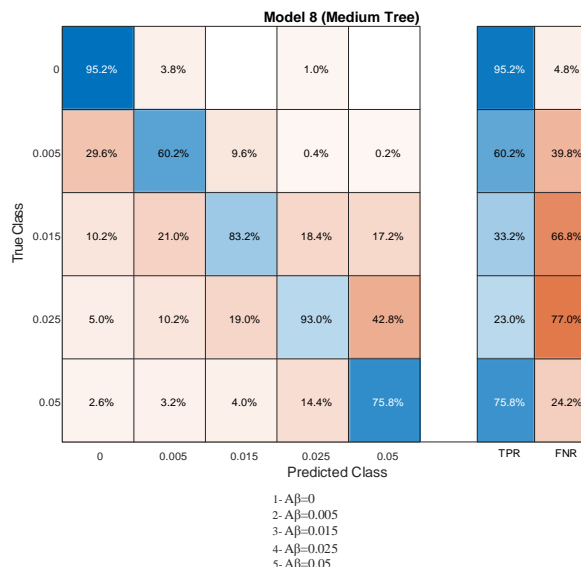


**Figure 4.** Confusion Matrix.

#### 4. Conclusion and Future work

A new LSTM-based MC model is suggested in this paper to improve the hitting probability of MMs. For the lowest number of Aβ values, the number of received molecules is obtained higher. Although the proposed model has the lowest number of Aβ values, the number of received molecules is higher because certain molecules are absorbed by the number of Aβ

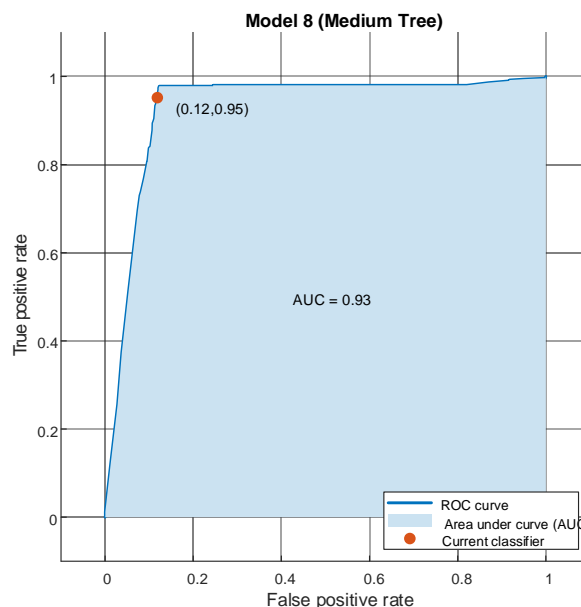


**Figure 5.** ROC Curve.

placed in the diffusion environment, which impacts communication quality. After obtaining the number of molecules received, the LSTM deep learning model was used to classify the number of Aβ values. More dynamic and biological systems can be constructed in the future by constructing a

proposed mobile MC model that takes into account more practical parameters such as precise drift velocity, vascular branching, and the influence of blood molecules. Also, using a deep neural network, estimate and optimization of the number of  $A\beta$  values in the environment can be considered to construct a more dynamic model with a lower signal to interference rate and a high receiver reception probability [28-30].

### Author Statements:

- **Ethical approval:** The conducted research is not related to either human or animal use.
- **Conflict of interest:** The authors declare that they have no known competing financial interests or personal relationships that could have appeared to influence the work reported in this paper
- **Acknowledgement:** The authors declare that they have nobody or no-company to acknowledge.
- **Author contributions:** The authors declare that they have equal right on this paper.
- **Funding information:** The authors declare that there is no funding to be acknowledged.
- **Data availability statement:** The data that support the findings of this study are available on request from the corresponding author. The data are not publicly available due to privacy or ethical restrictions.

### References

- [1] T. H. Yutaka Okaie, Shouhei Kobayashi Tadashi Nakano, Yasushi Hiraoka, Tokuko Haraguchi, (2019). Methods and Applications of Mobile Molecular Communication. *Proc. IEEE*, 107(7) doi: 10.1109/JPROC.2019.2917625.
- [2] Nariman Farsad, Weisi Guo†, Andrew Eckford (2014). Molecular Communication Link. Proceedings - IEEE INFOCOM DOI:10.1109/INFCOMW.2014.6849178 Conference: Computer Communications Workshops (INFOCOM WKSHPS), 2014 IEEE Conference on
- [3] Benmansour, Djazia Leila et al. (2019). The nano scale bending and dynamic properties of isolated protein microtubules based on modified strain gradient theory,” *Adv. Nano Res.*, 7(6):343-357 10.12989/anr.2019.7.6.443
- [4] Ismail Bensaid, Ismail Bensaid, Ahmed Bekhadda and Bachir Kerboua (2018). Dynamic analysis of higher order shear-deformable nanobeams resting on elastic foundation based on nonlocal strain gradient theory,” *Adv. Nano Res.*, 6(3):279-298 doi.org/10.12989/anr.2018.6.3.279
- [5] Wael A. Altabay, Mohammad Noori, Ali Alarjani and Ying Zhao (2020). Nano-delamination monitoring of BFRP nano-pipes of electrical potential change with ANNs. *Adv. Nano Res.*, 9(1):1-13 doi.org/10.12989/anr.2020.9.1.001
- [6] E. Isik and H. Toktamis, (2019). TLD characteristic of glass, feldspathic and lithium disilicate ceramics,” *Luminescence*, 34(2):272–279 doi: 10.1002/bio.3605.
- [7] H. B. Yilmaz, A. C. Heren, and T. Tugcu, (2014). 3-D Channel Characteristics for Molecular Communications with an Absorbing Receiver,” *IEEE Commun. Lett.* <https://arxiv.org/pdf/1404.4496.pdf>
- [8] Serena Lowa and Young-Seok Shon (2018). Molecular interactions between pre-formed metal nanoparticles and graphene families,” *Adv. Nano Res.*, 6(4):357-375.
- [9] E. Isik, (2020). Analyzing of the Viscosity by Using Artificial Neural Networks,” *J. Phys. Chem. Funct. Mater.* 3(2):72–76.
- [10] L. Lin, Q. Wu, M. Ma, and H. Yan, (2019). Concentration-based demodulation scheme for mobile receiver in molecular communication. *Nano Commun. Netw.*, 20:11–19 doi: 10.1016/j.nancom.2019.01.003.
- [11] S. Huang, L. Lin, W. Guo, H. Yan, J. Xu, and F. Liu, (2020). Initial Distance Estimation and Signal Detection for Diffusive Mobile Molecular Communication. *IEEE Trans. Nanobioscience*, vol. 19(3):422–433 doi: 10.1109/TNB.2020.2986314.
- [12] G. Wu and P. Tseng, (2021). A Deep Neural Network-Based Indoor Positioning Method using Channel State Information. pp. 290–294.
- [13] C. M. A. Niitsoo, T. Edelhäußer, E. Eberlein, N. Hadaschik. (2018). A Deep Learning Approach to Position Estimation from Channel Impulse Responses,” *Sensors*, 19(5):1064 doi: 10.3390/s19051064.
- [14] N. Farsad and A. Goldsmith, (2018). Neural Network Detectors for Sequence Detection in Communication Systems. <https://doi.org/10.1109/TSP.2018.2868322>
- [15] D. J. Selkoe *et al.* (1996). The role of APP processing and trafficking pathways in the formation of amyloid  $\beta$ -protein. *Ann. N. Y. Acad. Sci.*, 777(617):57–64. doi: 10.1111/j.1749-6632.1996.tb34401.x.
- [16] Y. Zhou *et al.*, (2017). Amyloid beta: structure, biology and structure-based therapeutic development,” *Acta Pharmacol. Sin.*, 38(9):1205–1235. doi: 10.1038/aps.2017.28.
- [17] M. T. Barros, W. Silva, and C. D. M. Regis, (2018). The Multi-Scale Impact of the Alzheimer’s Disease in the Topology Diversity of Astrocytes Molecular Communications Nanonetworks. Available: <http://arxiv.org/abs/1810.09294>.
- [18] H. A. Pearson and C. Peers, (2006). Physiological roles for amyloid  $\beta$  peptides. *The Journal of Physiology*. 1:5-10. doi: 10.1113/jphysiol.2006.111203.
- [19] Q. Wu, L. Lin, Z. Luo, and H. Yan, (2017). Bit alignment scheme for mobile receiver in molecular communication,” *Int. Conf. Ubiquitous Futur.*

- Networks, ICUFN*, pp. 750–752, doi: 10.1109/ICUFN.2017.7993892.
- [20] Walsh, Frank (2013) *Protocols for Molecular Communication Nanonetworks*. PhD thesis, Waterford Institute of Technology.
- [21] E. Isik, (2021). Analyzing of the diffusion constant on the nano-scale systems by using artificial neural networks,” *AIP Adv.*, 11(10) doi: 10.1063/5.0067795.
- [22] I. Isik, (2022). How Mobility of Transmitter and Receiver Effect the Communication Quality. *AIP Advances* 12(2):025205 DOI:10.1063/5.0082856
- [23] A. Tomar and N. Gupta (2020). Prediction for the spread of COVID-19 in India and effectiveness of preventive measures. *Sci. Total Environ.*, 728:138762doi:10.1016/J.SCITOTENV.2020.138762.
- [24] S. Hochreiter and J. Schmidhuber. (1997). Long Short-Term Memory. *Neural Comput.*, 9(8):1735–1780 doi: 10.1162/neco.1997.9.8.1735.
- [25] A. A. Chowdhury, K. T. Hasan, and K. K. S. Hoque. (2021). Analysis and Prediction of COVID-19 Pandemic in Bangladesh by Using ANFIS and LSTM Network. *Cognit. Comput.*, 13(3):761–770 doi: 10.1007/s12559-021-09859-0.
- [26] K.Vijayaprabakaran and K.Sathiyamurthy (2020). Towards activation function search for long short-term model network: A differential evolution based approach,” *J. King Saud Univ. - Comput. Inf. Sci.*, (in press) doi: <https://doi.org/10.1016/j.jksuci.2020.04.015>.
- [27] X. Glorot and Y. Bengio, (2010). *Understanding the difficulty of training deep feedforward neural networks*. Thirteenth international conference on artificial intelligence and statistics. 249–256.
- [28] M. B. Er, E. Isik, and I. Isik (2021). Parkinson’s detection based on combined CNN and LSTM using enhanced speech signals with Variational mode decomposition. *Biomed. Signal Process. Control* 70:103006 doi: 10.1016/J.BSPC.2021.103006
- [29] I. Isik, H. B. Yilmaz, and M. E. Tagluk, (2017 September 16-17). *A Preliminary Investigation of Receiver Models in Molecular Communication via Diffusion* [Conference presentation abstract]. 2nd International Conference on Artificial Intelligence and Data Processing (IDAP17), Malatya, Türkiye
- [30] E. Isik, I. Isik, and H. Toktamis, (2021). Analysis and estimation of fading time from thermoluminescence glow curve by using artificial neural network. *Radiat. Eff. Defects Solids* 176(9-10):765-776 doi: 10.1080/10420150.2021.1954000.